ICESat-2/ATLAS at 4 years: instrument performance and projected life

Anthony J. Martino*[a], John Cavanaugh[a], Aimee Gibbons[b], James E. Golder[c], Alvaro Ivanoff[d], Peggy Jester[b], Nathan Kurtz[a], Tom Neumann[a], Almut Pingel[e], Craig Swenson[e]

[a]NASA Goddard Space Flight Center, 8800 Greenbelt Rd., Greenbelt, MD 20771; [b]KBR Wyle; [c]Emergent Space Technologies; [d]Adnet Systems; [e]Science Systems and Applications

ABSTRACT

NASA's ICESat-2 mission launched in September 2018 carrying a single instrument, the Advanced Topographic Laser Altimeter System (ATLAS). ATLAS uses a high-repetition-rate, low-pulse-energy laser with its output split into six beams and a photon-counting receiver to measure Earth surface elevation with centimeter-level precision, repeating its ground track every 91 days. During more than four years of on-orbit operation, ATLAS has met or exceeded its lifetime and performance requirements. We present performance measurements, trends and projections for several instrument parameter, including transmitted laser pulse energy, receiver sensitivity, the instrument's impulse response, transmitter/receiver alignment, dead-time behavior, and elevation measurement performance.

The laser energy setting was increased in September 2023, for the first time, to maintain ranging performance at its early-mission level. The trends in instrument parameters indicate capability to continue on-orbit operation of ATLAS for many years into the future.

Keywords: ICESat-2, lidar, laser altimeter, photon-counting, remote sensing, cryospheric science

1. INTRODUCTION

NASA's ICE, Cloud, and land Elevation Satellite – 2 (ICESat-2)[1] was launched on 15 September 2018 from Vandenberg Air Force Base in California, USA. The primary science objectives of ICESat-2 include measurements of polar ice sheet elevation changes, sea ice freeboard, and vegetation canopy height globally[2]. The ICESat-2 observatory carries a single instrument: the Advanced Topographic Laser Altimeter System (ATLAS). ICESat-2 data products also enable studies of atmospheric profiles, ocean and inland water surfaces, land surfaces, and shallow-water bathymetry.

The ICESat-2 mission was led by the NASA Goddard Space Flight Center (GSFC), with significant support from industry partners for key mission components during the design and implementation phases. During data collection, the mission continues to be managed by GSFC, with spacecraft operations led by Northrop Grumman Innovation Systems and data delivery through the National Snow and Ice Data Center (NSIDC). Data were first made available to the public in late May 2019, and to-date there are over 6280 data users of 19 data products derived from elevation measurements enabled by the ATLAS instrument.

ICESat-2 launched with a requirement for three years of orbital operation after a 60-day commissioning period. It has now completed more than four years of orbital operation and continues to meet its performance requirements. In this paper, we summarize the design of ATLAS, provide an assessment of the on-orbit performance of ATLAS, and project its future performance.

2. ATLAS INSTRUMENT DESIGN

The design of ATLAS, and its early-mission performance, were described in an earlier paper[3]. Here we summarize the key features.

ATLAS is a six-beam ATLAS laser altimeter that uses 532 nm laser light and single-photon sensitive detectors to measure the two-way travel time of individual photons between the instrument and a target. Its major elements are shown in Figure 1. Functionally, ATLAS consists of a transmitter that sends out laser pulses in 6 beams, a receiver that collects returned light and sends it into 6 independent photon detection/counting/timing chains, and an alignment monitor/control system that keeps the transmitted beams pointed where the receiver is looking and reports the pointing directions of the transmitted beams.

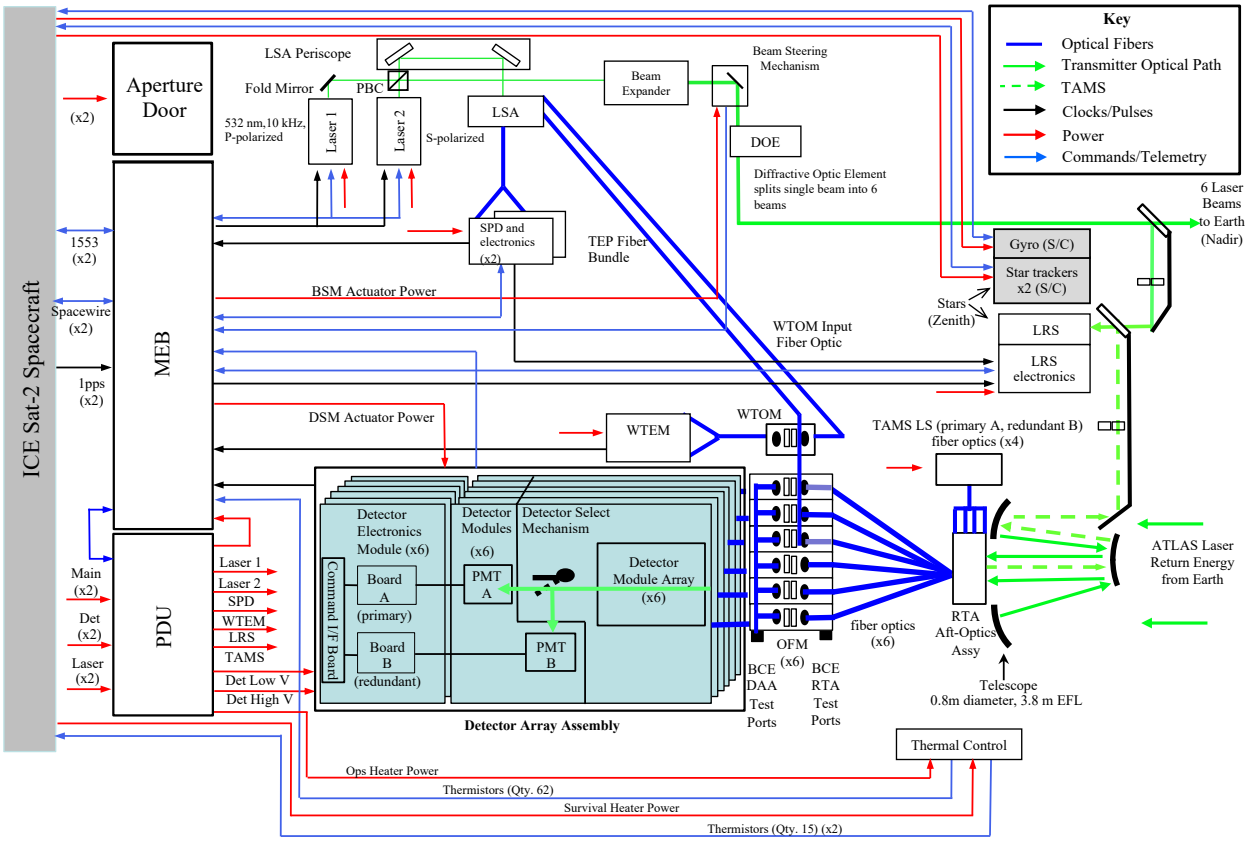

Figure 1. Functional Diagram of the ATLAS instrument.

The transmitter includes a primary and a redundant laser and beam-forming optics. The frequency-doubled Nd:YVO_4 laser fires at 10 kHz with a FWHM pulse width approximately 1.3 ns and pulse energy commandable in 11 steps between 250 and 1400 μJ. A small fraction of the energy is sampled for internal use within the instrument. The rest goes through a reflective beam expander. The expanded beam reflects off a beam-steering mirror and then passes through a diffractive optical element that splits 80% of the energy into 6 useful beams; the remaining 20% is divided between undiffracted light and numerous other diffracted orders. The beams are sampled by the beamsplitter face of a lateral transfer retroreflector; most of the energy then propagates out of the instrument.

The six useful beams illuminate a rectangular pattern on the ground (Figure 2.) The direction of travel is at a slight angle to the short side of the rectangle, so the tracks of the beams form three closely-spaced pairs. Each pair gives the cross-track slope in the vicinity of the measurement, addressing a need that was identified by ICESat. Within each pair, one beam (the "strong" beam) has four times the pulse energy of the other; this was the result of trading probability of getting a slope measurement against probability of getting at least a single height measurement.

The receiver telescope's focal plane contains images of the spots on the Earth's surface illuminated by the six laser beams; with proper alignment, each of the image spots is captured by its own optical fiber, which acts as a field stop. After filtering to reduce solar background light, each spot is coupled by its own optical fiber to a photon-counting detector that produces a digital edge for each photon detection event. Individual events are timed with approximately 200 ps precision, and on-board software selects for telemetry those events that are determined to be within a band around the surface. In addition, an "atmospheric histogram" is telemetered, containing counts of events in 200 ns bins accumulated over 400 laser shots.

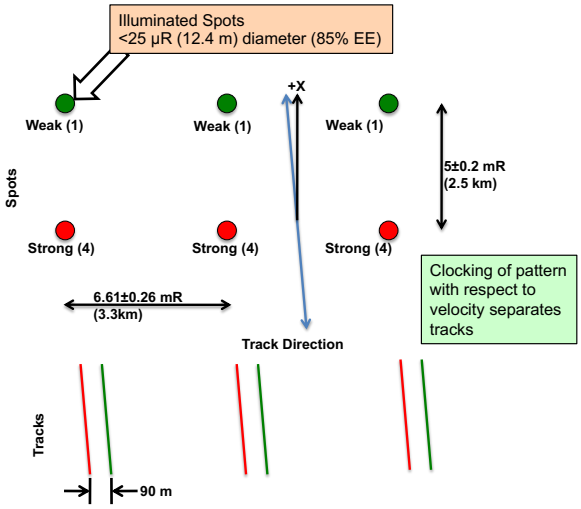

Figure 2. Transmitted beam pattern. ATLAS illuminates six spots on the ground in a rectangular pattern, at a slight angle to the direction of travel, resulting in three pairs of tracks.

The energy sampled from the raw laser beam is used for three purposes: timing, wavelength tracking, and instrument characterization. Some of the energy illuminates an analog Start Pulse Detector; threshold-crossing signals are sent to the same timing electronics as are used for photon detection events to provide a start time for the eventual time-of-flight calculations. Another part of the energy is fed, suitably attenuated, into the receiver optical paths for two of the beams, just ahead of their solar-blocking filters; this provides a means to monitor changes to the instrument's impulse response and timing bias. Finally, a part of the energy is put through a copy of the solar-blocking filters, on and off axis, to monitor the relative tuning between the laser and the filters.

The retroreflected beam samples are imaged onto a camera in the Laser Reference System (LRS), suitably defocused to allow sub-pixel centroiding. Four spots in the telescope focal plane are back-illuminated at a slightly different wavelength; the resulting beams coming out of the telescope are retroreflected and imaged onto the same camera. On-board software uses the centroids of the laser spots and telescope spots to determine the alignment offset between the transmitted beams and the receiver fields of view, and, if necessary, commands the beam steering mechanism (BSM) to move, maintaining transmitter/receiver alignment. This active alignment scheme was deemed necessary because both the beam divergence and the field-of-view diameter are much smaller than on any previous spaceborne laser altimeters, leaving much less margin for misalignment. Alignment shifts were seen during thermal-vacuum testing that, if not corrected by the control loop, would have resulted in severe losses of throughput.

The telemetry from ATLAS includes laser fire times, photon detection times, atmospheric histograms, and spot centroids, as well as hundreds of other instrument parameters. These data are turned into time of flight, then range, and pointing direction, by the ground system, finally yielding geolocated elevation for each photon detection event.

Table 1. Nominal values of key ATLAS instrument parameters. Values vary from beam to beam, and with temperature; typical values are given here.

Parameter Name	Value	Units
Laser Firing Rate	10	kHz
Transmitted Energy (strong beam)	48 to 172	μJ
Transmitted Energy (weak beam)	12 to 43	μJ
Transmitted Wavelength	532.272	nm
Transmitted Beam divergence (85% enclosed energy)	24	μR
Transmitted Beam Eccentricity	0.4	none
Transmitted Beam Angular Spacing (long dimension)	6.6	mR
Transmitted Beam Angular Spacing (short dimension)	5	mR
Receiver Aperture Diameter	0.802	m
Receiver Aperture Effective Area	0.41	m^2
Receiver Field of View Angular Diameter	83.5	μR
Receiver Optical Throughput (at peak wavelength; does not include obstruction in telescope)	0.41	none
Receiver Counting Efficiency	0.15	none
Receiver Effective Optical Bandwidth	38	pm
Event timing precision	200	ps
Single-photon time-of-flight uncertainty (standard deviation)	800	ps

3. TRANSMITTER ON-ORBIT PERFORMANCE

ATLAS has operated, for the entire mission so far, using Laser 2 only. Laser 1 has been held in reserve.

The performance of the transmitter is characterized here by two parameters: the pulse energy and the beam divergence.

3.1 Pulse Energy

At the beginning of instrument commissioning on orbit, the laser was set to Energy Level 6, corresponding to a total pulse energy of 630 μJ at the laser output and transmitted pulse energy of approximately 126 μJ in each strong beam. After the initial surface returns were evaluated, it was determined that a lower setting was needed to achieved the desired value of return strength. The laser setting was changed to Energy Level 4, corresponding to total pulse energy of 480 μJ and pulse energy of approximately 100 μJ in each strong beam. The setting remained at 4 until it was raised to 5 in September of 2022 to compensate for the effects of aging in the laser and receiver.

Figure 3 shows the total transmitted laser pulse energy, as measured by the laser's internal energy monitor and calibrated by pre-launch measurements. The energy tends to drift around with variations in the temperatures of the volume Bragg grating (VBG) that determines the laser wavelength and the second harmonic generator (SHG) that converts the laser's 1064-nm output to 532 nm. The VBG temperature is periodically readjusted to keep the laser wavelength at the center

wavelength of the receiver's passband, and the SHG temperature is periodically adjusted to keep the pulse energy at its maximal value for the energy setting. There is also a slow overall downward trend between 1% and 2% per year.

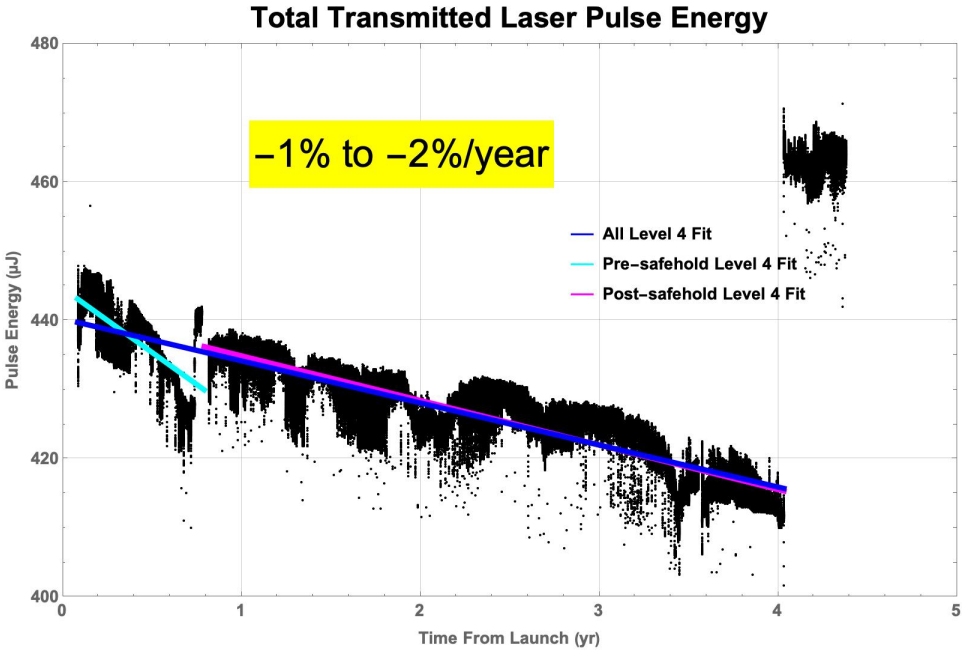

Figure 3. Transmitted energy. The total energy transmitted by ATLAS per pulse over the first 4+ years of the mission.

The increase in energy shortly after the 4-year point is due to changing the laser setting to Energy Level 5. There is not yet sufficient data to determine a trend at that setting.

3.2 Beam Divergence

The divergence of the ATLAS laser beams was measured before launch to be between 20 and 25 μR, with a nearly circular Gaussian shape, at most temperatures tested. At extreme cold temperatures, a more elliptical shape was observed, with the long axis nearly 35 μR. The temperatures observed on orbit are consistent with the nearly circular shape.

ATLAS does not have the internal capability to measure beam divergence on orbit. However, the spot size on the ground has been evaluated[4] using returns from an array of small retroreflectors at White Sands Missile Range in New Mexico, resulting in an estimated diameter of 10.9 ±1.2 m. This corresponds to a beam divergence of approximately 22 μR.

4. RECEIVER ON-ORBIT PERFORMANCE

The most important parameter for trending the receiver's radiometric performance is its responsivity. Combined with the transmitted energy, it determines the strength of the signals used for range measurement.

Multiple methods are available to evaluate the responsivity of the receiver; in some of these methods, the receiver and transmitter performance are coupled. Analysis of the background photon detection rate and of the return strength can be performed for all six beams; these are described here. In addition, an internal calibration path leads from the transmitter directly to the receiver for Beams 1 and 3; this is not discussed here.

Analysis of the background photon detection rate is the only method available on orbit that does not depend on knowledge of the transmitted pulse energy. The background rate is almost entirely due to sunlight scattered from the Earth within the

receiver's optical passband; the dark rates for all of the detectors are less than 10,000 s^{-1} except within the South Atlantic Anomaly, where they can reach 50,000 s^{-1}.

The amount of scattered solar light is highly dependent on the elevation of the sun above the horizon and the albedo of the scattering surface. To minimize the variation due to sun elevation, we selected a sample of data granules in which the sun elevation was within each of six 10-degree bands. Within each band, we minimized the variation due to albedo by finding the maximum value of background rate, which we assumed to represent scattering from thick clouds or bright snow. The results for Spot 1 are shown in Figure 4.

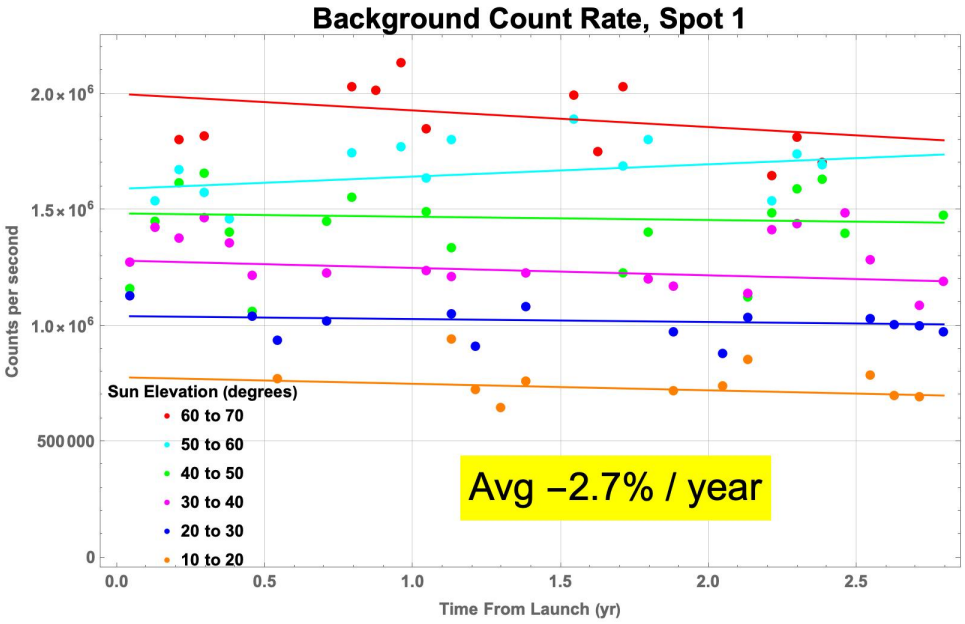

Figure 4. Background trend. The maximum background rate for one of the six spots during the first 3 years of the mission, for each range of sun elevation angle.

For each combination of spot and sun elevation, we determined a slope; the mean slope over all combinations was -2.7% per year. The variation of the slope values among the combinations was quite large, sometimes yielding a positive value; this is likely due to the sparse sampling. Therefore the uncertainty in the mean value is large.

The key radiometric performance parameter that determines the ability of ATLAS to make precise range measurements is the return strength. The instrument was designed to provide a mean value of 12 photoelectrons per shot in each strong beam in a return from a clean snow surface under a clear sky; this value provides the best ranging uncertainty without excessive distortion due the dead time of the photon-counting detectors.

Trends in return strength are monitored[5] by analyzing the returns from cloud-free areas of the interior of Antarctica, which provices a reliably large area of nearly-uniform albedo. Solar background is removed, as well as any data that shows distortion characteristic of saturated returns from specular reflections. The results are shown in Figure 5.

Slopes for each spot, calculated for the time period when the laser was at Energy Level 4, were between 2.0% and 3.4% per year, with a mean of -2.7% per year. Given the -1.5% per year trend in transmitted energy, this implies a lower rate of decline in responsivity than the mean value obtained from analysis of the background rates. The discrepancy may be

due to the high uncertainty in the result of the background analysis or to inherent biases in the methods used to separate return and background photon detection events.

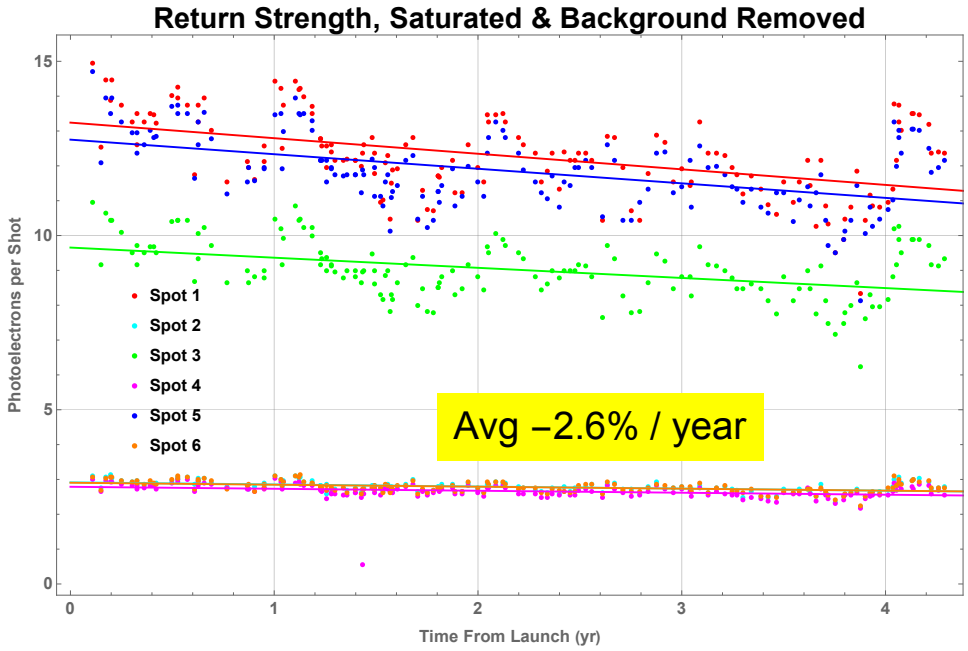

Figure 5. Antarctic return strength. Return photoelectrons per shot from areas that are selected to represent the design conditions, showing a downward trend over the first 4+ years of the mission.

5. ADJUSTMENT OF LASER ENERGY SETTING

The design target value for return strength was 12 photoelectrons per laser shot in each strong beam's return from a snow surface under a clear sky. This represents a compromise between a high signal-to-noise ratio and minimal biases due to distortion of the time-of-flight distribution arising from dead-time effects in the photon-counting receivers. On the basis of pre-launch target modeling and instrument calibration measurements, it was expected that this value would be obtained with the laser set to Energy Level 4. At the beginning of the post-launch commissioning period, the laser was set to Energy Level 6 to increase the likelihood of getting a detectable return before the instrument settings were optimized. Once the initial returns were analyzed, the laser was set to Energy Level 4. As is seen at the left side of Figure 5, two of the strong beams yielded return strengths slightly above the target value, and one yielded a return strength slightly below the target value. The team determined that this performance was acceptable, and the laser was left at Energy Level 4.

The strategy adopted during the mission design phase was to start with the laser energy at a low value and increase it from time to time to maintain consistent return strength throughout the mission. As the mission approached four years of orbital operation, the observed decline in return strength approached the point at which it would be returned to its early-mission value by increasing the laser's energy setting by one step. Accordingly, the laser setting was increased to Energy Level 5 in September 2022, just after four years in orbit. The jump in transmitted energy can be seen in Figure 3, and the resulting jump in return strength can be seen in Figure 5.

We expect to follow the strategy of increasing the laser energy setting by one step whenever such an increase would restore the return strength to its early-mission value. The predicted results of following this strategy are shown in Figure 6. Return strength relative to the early-mission value is shown for various assumptions regarding the rates at which laser energy and receiver responsivity decline as the laser energy is increased, compared to the projected return strength if the laser were left at Energy Level 4. Depending on the assumption, the laser setting would reach Energy Level 11 (the highest available)

between 16 and 21 years after launch, and would drop permanently to 90% of the early-mission value between 17 and 24 years after launch. This suggests that ATLAS could continue operating with its current performance until the late 2030s.

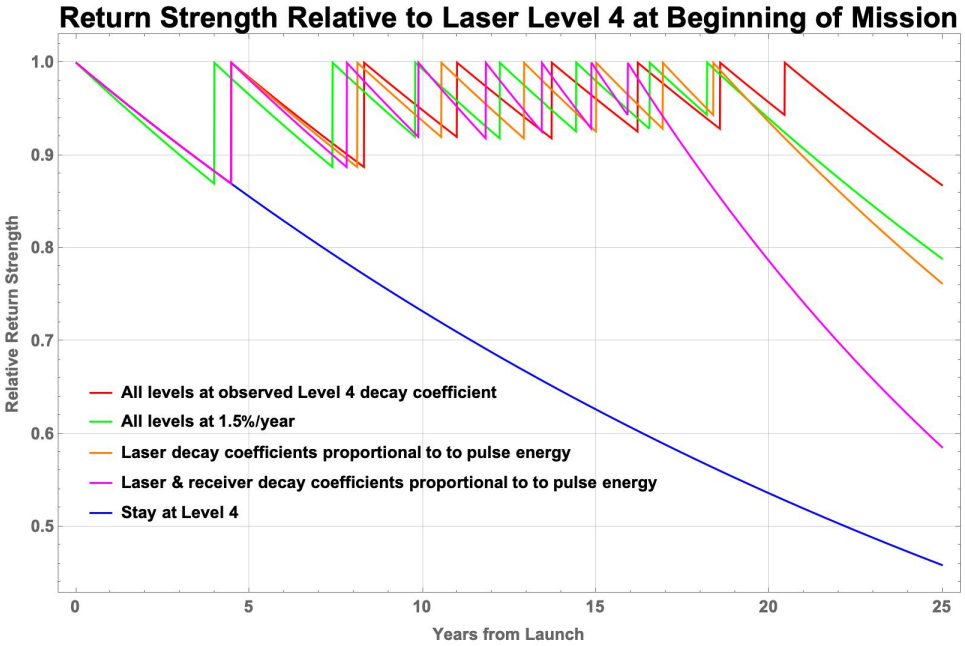

Figure 6. Projected return strength. Laser energy is increased by one step whenever that would restore the return strength to its early-mission value.

6. INSTRUMENT IMPULSE RESPONSE

The impulse response of ATLAS (the theoretical return from a flat, smooth surface perpendicular to the laser beam) is dominated by the shape of the transmitted pulse, but is also influenced by the optical and electronic behaviour of the receiver. When the number of photons in the return is low enough that few detection events are lost in the receiver's dead time, the instrument behaves as a linear system with a well-defined impulse response. At higher signal levels, such as those obtained from quasi-specular reflections, significant distortion can be observed.

6.1 Linear impulse response

The ATLAS impulse response was initially characterized before launch using returns from retroreflectors, attenuated to stay within the linear regime. After launch, features were observed in quasi-specular returns that had not been noticed in pre-launch testing. To a limited extent, it was possible to determine that some of these features also existed at a very low level in the linear impulse response by re-examining pre-launch data, but the test conditions made it difficult to characterize them accurately. To make an accurate characterization possible, we evaluated the linear impulse response from on-orbit data.

To approximate a flat, smooth surface, we chose a large salt flat – the Salar de Uyuni, in Bolivia. In addition to being large and nearly flat, its reflectance during the dry season is high enough to provide a large set of return photons, but not so high as to show significant distortion due to dead time. Numerous passes over this feature were available, with each pass tens of km long. In total, some 58 million photon detection events were included in the data set; this many were needed to clearly see features that are several orders of magnitude less prominent than the main peak. We removed the

large-scale surface relief in each pass before aligning the main peak in each pass and aggregating the data from all passes. After computing a histogram of time of flight relative to the time of flight for the main peak, we adjusted each histogram bin to compensate for the fact that data contributing to some of the far-off bins was not available from all passes. The result is shown in Figure 7.

In addition to the main (highest) peak (which would ideally be the only feature), two prominent "afterpulses" are seen with peak heights about 10^{-3} that of the main peak, plus a third "afterpulse" and a wide feature barely above the noise at 10^{-5} of the main peak height. These features are not typically visible in returns used for most scientific purposes because the number of events used is typically too small, but they are often visible in the highly-saturated returns due to quasi-specular reflections off of flat water surfaces.

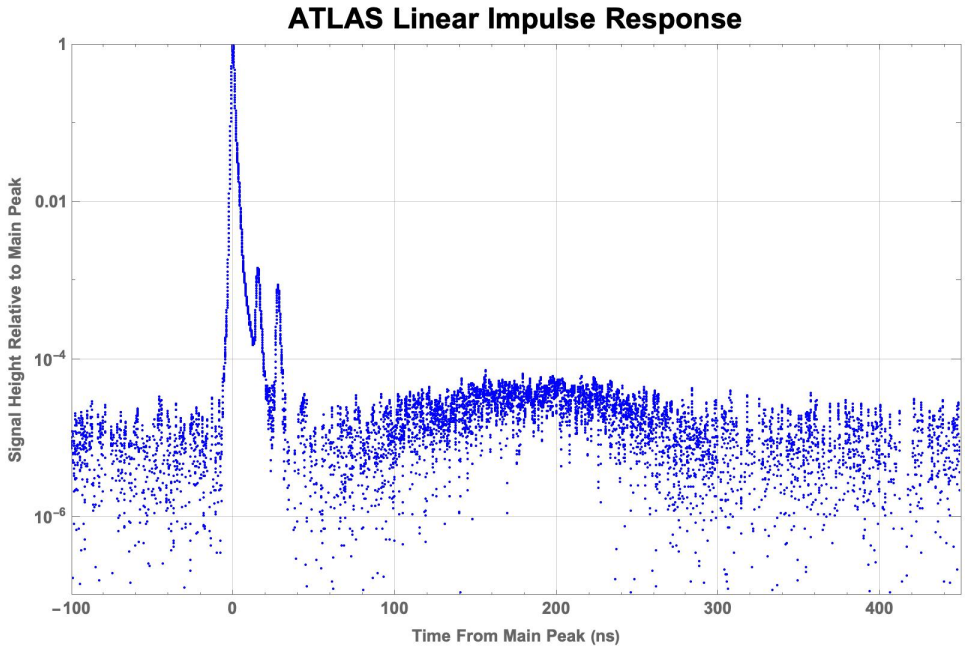

Figure 7. ATLAS linear impulse response. Obtained by analysis of returns from passes over Salar de Uyuni salt flats in Bolivia.

By tracing rays, we determined the sources of the "afterpulses" to be reflections within the receiver optics, as shown in Figure 8. Multiple reflections between surfaces of optical fibers, a beamsplitter (BS), solar-blocking filters, and the window of the photomultiplier tube (PMT) give rise to faint, delayed copies of the return pulse. These appear both in the surface return (shown in blue and green, entering through the telescope) and the Transmitter Echo Pulse (TEP) (shown in red and orange, entering through an optical fiber from the transmitter as shown in Figure 1). The observed locations and

heights of the afterpulses match well with the locations and heights predicted by the ray trace. In some cases, two or more multiple-reflection paths have nearly the same length, causing two or more "afterpulses" to appear as one.

We suspect that the wide feature after the third afterpulse originates within the photomultiplier tube.

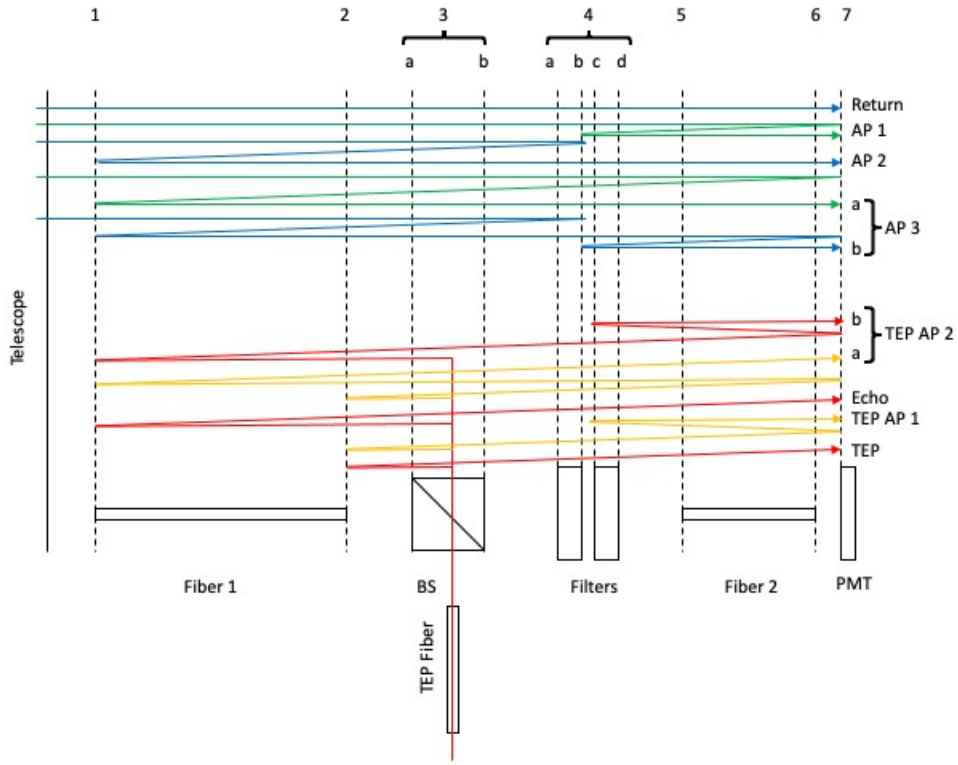

Figure 8. Source of extra pulses. Multiple reflections within the receiver optics produce delayed, highly-attenuated copies of the main pulse.

6.2 Dead time effects

Within the ATLAS receiver, there are 16 timing channels for each strong spot and 4 timing channels for each weak spot. Each timing channel exhibits paralyzable dead-time behavior within its initial analog stage and non-paralyzable dead-time behavior within its digital stage. The overall dead time for each channel is between 2.8 and 3.2 ns. In returns from most surfaces, the number of photoelectrons is small enough, and the photoelectrons are spread out enough in time (the distribution widens by about 6 ns per meter of relief), that few photoelectrons occur in a channel that has had a photoectron within the previous 3 ns. The small "first-photon" timing bias in most returns is easily corrected. However, quasi-specular returns result in so many photoelectrons occuring within a few nanoseconds that most of them are lost. The resulting distribution is highly skewed toward shorter times of flight (higher elevations) and may exhibit features that are not present

in the linear impulse response. Figure 9 shows a particularly striking example of this phenomenon. An effort is under way to model these returns, with the objective of correcting for their large "first-photon" bias.

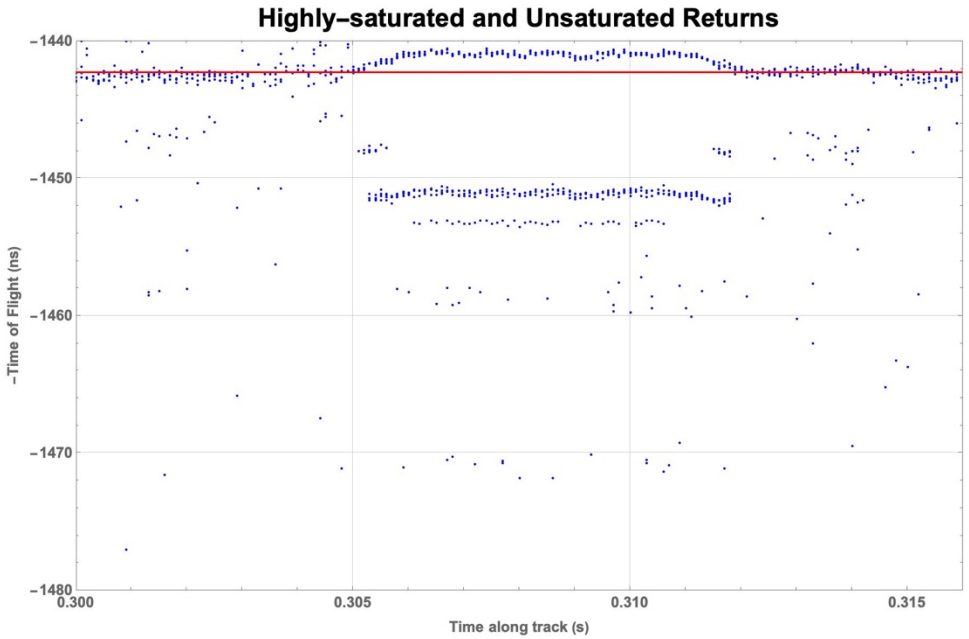

Figure 9. Highly saturated return. A highly-saturated return from a quasi-specular reflection between regions of unsaturated returns, showing linear "afterpulses" and dead time effects.

7. POINTING AND ALIGNMENT

The absolute pointing of ATLAS is determined using the laser-side camera of the LRS, which images samples of the transmitted beams, and the spacecraft's star trackers, which are mounted on the ATLAS optical bench along with the spacecraft's inertial reference unit. Mounting these spacecraft components on the ATLAS optical bench, rather than on the spacecraft bus, provides a much tighter mechanical coupling between them and the critical instrument components; this allow much more precise knowledge and control of the instrument's pointing. This design choice enabled the mission to meet its pointing requirements while using the spacecraft star trackers as a substitute for a stellar camera within the LRS, which exhibited severe stray-light artifacts on orbit.

The transmitted beams must be kept pointed at the areas on the earth surface covered by the receiver's six fields of view to within less than 35 μR to avoid clipping of the illuminated spot by the edge of the FOV, which would result loss of signal, geolocation error, and potentially an elevation bias on sloped surfaces.

In normal operation, the control loop described in Section 1, using the LRS and the BSM, keeps the transmitter/receiver angle within less than 3 μR of the set point. During scheduled calibrations, the control loop is opened, and the BSM is either held in a fixed position or swept back and forth across the field of view.

Once a month, a "stare" calibration is performed in which the BSM is held at a fixed position for slightly more than two orbital periods. (At the same time, the receiver's timing window is adjusted to constantly capture photon detection events from the internal calibration path (TEP) rather than the surface return.) Figure 10 and Figure 11 show the behavior of the offset angle between the transmitter and receiver, as measured by the LRS laser camera, during "stare" calibrations on three dates: 2020-09-11, 2021-01-16, and 2021-04-09. Figure 10 shows the two-dimensional spatial patterns; the motion occurs roughly along a line at 45˚ to both axes. Figure 11 shows the temporal behavior with the two-dimensional offset projected on a line at 45˚ to both axes.

On 2020-09-11 (orange), the angle between the orbital plane and the sun vector (Beta angle) was such that ICESat-2 was illuminated by the sun throughout its orbit. On the other two dates, the Beta angle was such that ICESat-2 was in eclipse for part of its orbit. The difference is evident in the overall range of motion shown in Figure 10, and in the periodic behavior seen in Figure 11.

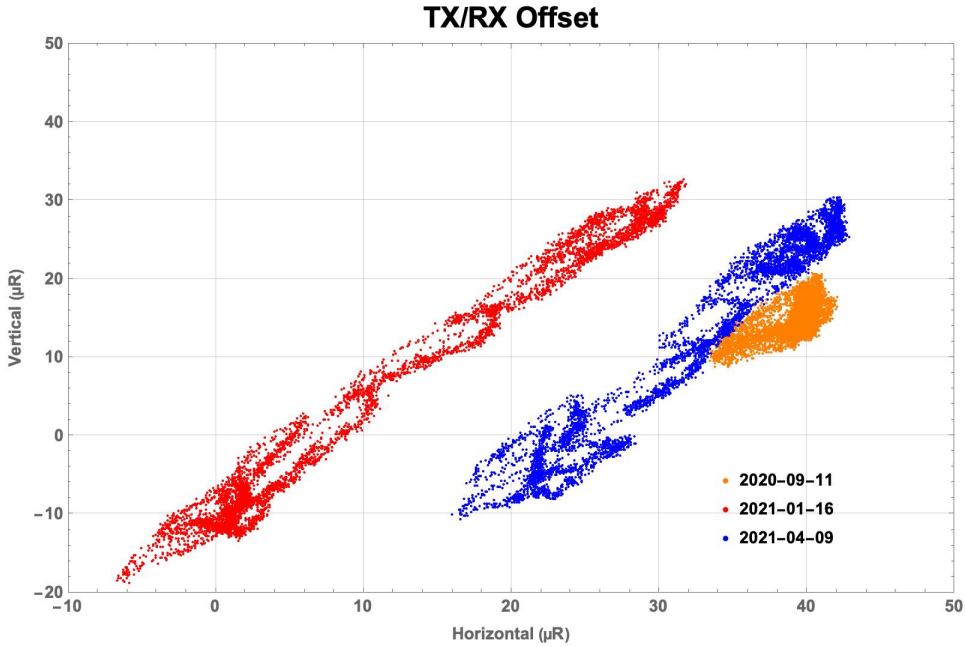

Figure 10. Spatial behavior of TX/RX offset with BSM frozen.

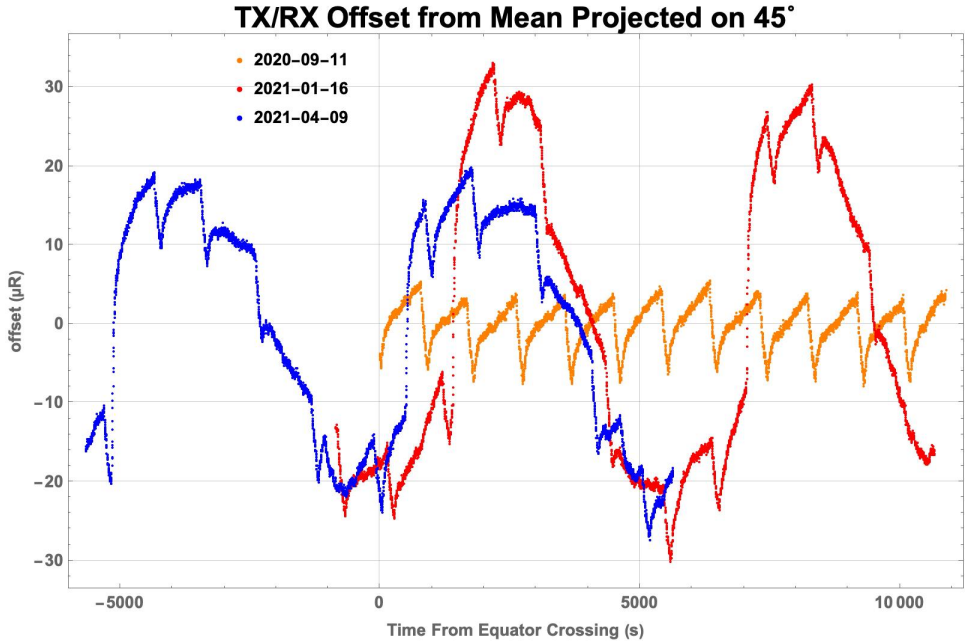

Figure 11. Temporal behavior of TX/RX offset with BSM frozen.

On the dates when ICESat-2 went in and out of eclipse during each orbit, a large oscillation (up to 60 μR peak-to-peak) is seen at the orbital period, with a faster oscillation superimposed on it. This oscillation is large enough that the laser-illuminated spots would be severely clipped by the edge of the FOV if the control loop were not in operation.

On the date when ICESat-2 did not go into eclipse, only the smaller, faster oscillation is seen. This oscillation is due to a heater cycling on and off.

At least once per day, a calibration is performed in which the BSM sweeps the transmitted beams completely across the receiver FOV many times per second, for about 30 seconds parallel to each axis. The strength of the surface return is analyzed as a function of the TX/RX offset angle, and the "optimal" offset is determined as the center of the region in the middle of the FOV where the return strength is nearly constant. The results of this calibration over the mission time are shown in Figure 12.

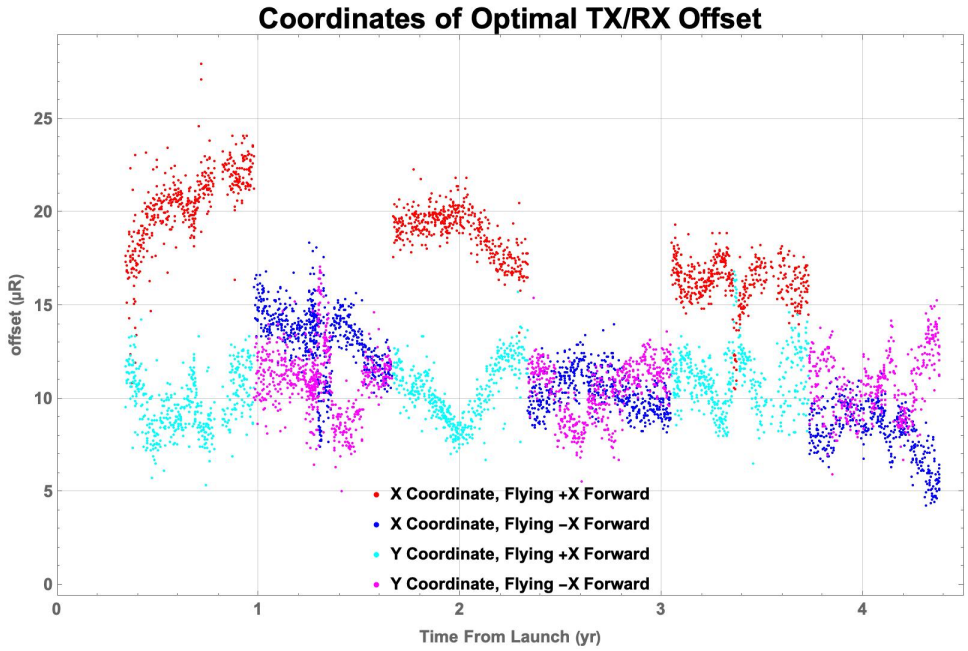

Figure 12. Result of field-of-view sweep over time. The optimal transmit/receive offset angle is driven primarily by the spacecraft orientation, with a slow trend also appearing in the X coordinate.

While the Y coordinate is constant to within less than ±5 μR over the mission, the X coordinate shows a distinct dependence on the orientation of ICESat-2 relative to the velocity vector. The X coordinate changes by about 10 μR each time the observatory performs a "yaw flip" maneuver, which is done approximately every 9 months to keep the solar arrays and radiators properly oriented relative to the sun and deep space.

Early in the mission, the instrument team adjusted the set point for the alignment control loop every few weeks to keep up with the results of the FOV sweeps. Once the consistent behavior shown in Figure 12 was confirmed, the team began changing the set point only after each "yaw flip" to reduce the potential for creating artifacts.

8. ELEVATION MEASUREMENT

Timing, pointing, and spacecraft position data, as well as engineering data, are downlinked from ICESat-2 and processed by the ground system into numerous data products. In ATL02[6], the lowest-level publicly available data set, timing data are converted into range measurements, and all ATLAS instrument calibrations are applied.

The fundamental science data product published by the ICESat-2 mission, ATL03[7], contains geolocated "photon" heights: latitude, longitude, and elevation (relative to a reference ellipsoid somewhere near sea level) for each photon detection event. ATL03 is then processed into more specialized data products optimized for land ice, sea ice, vegetation, and other areas of scientific study.

Figure 13 and Figure 14 show examples of ATL03 data, in which elevations of "photons" are plotted against position on the Earth suface, demonstrating the measurement capabilities of ICESat-2 and ATLAS. Figure 13 shows a profile collected

during a pass over Hutt Lagoon on the Indian Ocean coast of Western Australia. Note that the reference ellipsoid height is between 20 and 25 meters above the observed sea level at this time and place. In the lagoon, the surface of which is below sea level, enclosures are used in connection with the commercial growth and harvesting of algae; the corner of one such enclosure is visible in the figure less than a meter above the water surface. The ocean water is clear enough that the underwater portion of the off-shore reef is visible, and the rough ocean surface can be contrasted with the smooth surface of the lagoon. In this night-time pass, very little background is observed.

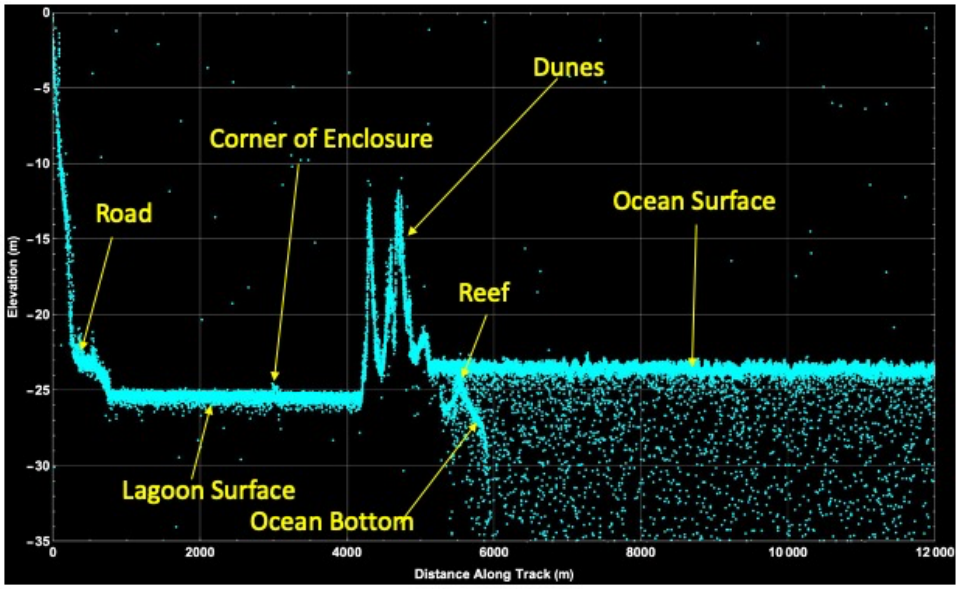

Figure 13. Elevation profile of Hutt Lagoon, Western Australia. Coastal hills, lagoon surface, dunes, ocean surface and near-shore bottom are visible. Data file ATL03_20200813115539_07500809_005_01.h5.

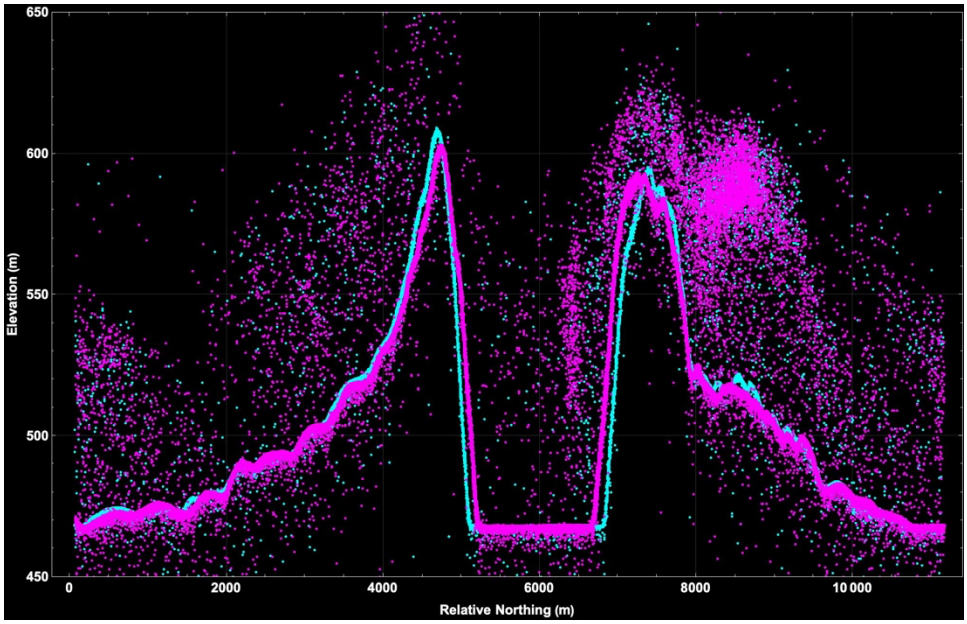

Figure 14. Elevation profiles of Pingaluit Crater, Quebec, Canada. Profiles from a strong beam (cyan) and its adjacent weak beam (magenta) show the crater walls, lake surface at the bottom, and ground fog. Data from file ATL03_20210330012232_00801103_004_01.h5.

Figure 14 shows data from a pass over Pingaluit Crater, a nearly-circular water-filled meteorite impact feature in northern Quebec. This is also a night-time pass, but there is noticeable return from ground fog, particularly on the north side of the

crater. Dual profiles from a strong beam and a weak beam, 90 meters apart, show similar terrain and atmospheric properties, with the expected narrowing of the feature farther from its center.

Data from ICESat-2 have provided the basis for at least 326 scientific papers to date.

9. CONCLUSION

The ATLAS instrument on ICESat-2 continues to meet or exceed its performance requirements after more than four years of orbital operation. The observed trends point to a slow degradation of instrument performance, allowing it to meet its performance requirements well into the next decade.

REFERENCES

[1] Markus, T., Neumann, T., Martino, A. J., K., Abdalati, W., Brunt, K., Csatho, B., Farrell, S., Fricker, H., Gardner, A., Harding, D., Jasinski, M., Kwok, R., Magruder, L., Lubin, D., Luthcke, S., Morison, J., Nelson, R., Neuenschwander, A., Palm, S., Popescu, S., Shum, C.K., Schutz, B.E., Smith, B., Yang, Y., Zwally, H.J., "The Ice, Cloud and land Elevation Satellite-2 (ICESat-2): Science requirements, concept, and implementation," Remote Sensing of the Environment, 190, 260-273, doi: 10.1016/j.rse.2016.12.029 (2017).

[2] Neumann, T., Martino, A. J., Markus, T., Bae, S., Bock, M., Brenner, A., Brunt, K., Cavanaugh, J., Fernandes, S., Hancock, D., Harbeck, K., Lee, J., Kurtz, N., Luers, P., Luthcke, S., Magruder, L., Pennington, T., Ramos-Izquierdo, L., Rebold, T., Skoog, J., Thomas, T., "The Ice, Cloud, and Land Elevation Satellite -2 Mission: A Global Geolocated Photon Product Derived From the Advanced topographic Laser Altimeter System,", Remote Sensing of the Environment, doi:10.1016/j.rse.2019.111325 (2019).

[3] Anthony J. Martino, Thomas A. Neumann, Nathan T. Kurtz, Douglas McLennan, "ICESat-2 mission overview and early performance," Proc. SPIE 11151, Sensors, Systems, and Next-Generation Satellites XXIII, 111510C (10 October 2019); doi: 10.1117/12.2534938.

[4] Magruder, L., Brunt, K., Neumann, T., Klotz, B., & Alonzo, M. (2021). Passive ground-based optical techniques for monitoring the on-orbit ICESat-2 altimeter geolocation and footprint diameter. Earth and Space Science, 8, e2020EA001414. https://doi.org/10.1029/2020EA001414.

[5] Gibbons, A., Neumann, T., Hancock, D., Harbeck, K., & Lee, J. (2021). On-orbit radiometric performance on ICESat-2. Earth and Space Science, 8, e2020EA001503. https://doi.org/10.1029/2020EA001503.

[6] Martino, A. J., M. R. Bock, C. Gosmeyer, C. Field, T. A. Neumann, D. Hancock, R. L. Jones III, P. W. Dabney, C. E. Webb, and J. Lee. (2021). ATLAS/ICESat-2 L1B Converted Telemetry Data, Version 5. Boulder, Colorado USA. NASA National Snow and Ice Data Center Distributed Active Archive Center. https://doi.org/10.5067/ATLAS/ATL02.005.

[7] Neumann, T. A., A. Brenner, D. Hancock, J. Robbins, J. Saba, K. Harbeck, A. Gibbons, J. Lee, S. B. Luthcke, T. Rebold, et al. 2021. ATLAS/ICESat-2 L2A Global Geolocated Photon Data, Version 5. Boulder, Colorado USA. NASA National Snow and Ice Data Center Distributed Active Archive Center. https://doi.org/10.5067/ATLAS/ATL03.005.